

Hydrocarbon and Soot Oxidation over Cerium and Iron Doped Vanadium SCR Catalysts

Lei Zheng,^[a] Anna Zimina,^[a, b] Maria Casapu,^{*,[a]} and Jan-Dierk Grunwaldt^[a, b]

V₂O₅–WO₃/TiO₂ (VWTi) catalysts are widely employed for selective catalytic reduction (SCR) of NO_x. However, due to their poor thermal stability the application in diesel particulate filters (DPFs), *i.e.* 2-way SCR on DPF is limited. In this study, the potential of Ce- and Fe-doped VWTi systems for hydrocarbon and soot oxidation in addition to the SCR activity was systematically investigated for fresh and thermally aged samples. The formation of metal vanadates upon thermal aging, as identified by X-ray diffraction, Raman and X-ray adsorption spectroscopy, prevents drastic sintering of the support and maintains a high

NO_x-SCR and hydrocarbon oxidation activity. Additionally, the doped VWTi catalysts show a slight increase of the CO₂ selectivity during hydrocarbon oxidation, which represents an important aspect for such multifunctional catalysts. Despite of the advantages, the formation of metal vanadates hinders the mobility of vanadium species and decreases the soot oxidation ability of the doped catalysts. Interestingly, a promising soot oxidation activity was identified for the VWTi–Fe sample after aging at 650 °C, which resulted in decomposition of the iron vanadate and generation of highly dispersed and mobile V₂O₅.

1. Introduction

Selective catalytic reduction (SCR) of NO_x with ammonia is to date one of the most widespread technologies for NO_x abatement particularly for heavy-duty diesel engines.^[1] Vanadium-based SCR catalysts (V-SCR), typically containing vanadium as redox active species and tungsten to reinforce TiO₂ as support (V₂O₅–WO₃/TiO₂),^[2] are widely used for NO_x reduction due to their good removal efficiency and high resistance against sulfur-poisoning.^[1b] However, particularly the poor thermal stability of vanadia^[3] represents a significant challenge due to the dynamic temperature changes encountered for mobile applications. Chapman *et al.*^[4] demonstrated that V₂O₅ is released already at around 550 °C, which strongly limits their high temperature application. In order to overcome this problem different solutions have been proposed, including the use of V-free TiO₂- or WO₃-based catalysts.^[5] Recent studies have shown that metal vanadates based SCR catalysts are promising alternatives, which could be used to prevent vanadium volatilization. Particularly, cerium, iron and erbium vanadates exhibit enhanced thermal stability during SCR

reactions by stabilizing the vanadium species and inhibiting the sintering tendency while maintaining a good NO_x removal activity.^[6] Due to their higher thermal durability and good SO₂ poisoning resistance,^[6d,f,7] such catalyst formulations seem to be suitable also for 2-way SCR on DPF (or SDPF) catalyst applications.^[8] For such combinations of the NO_x-SCR and particulate matter filtration functionalities the exposure to high temperatures is highly probable during DPF regeneration and because this exhaust gas aftertreatment component is located closer to the engine.^[9] Hereof, an enhanced SCR performance was observed over Ce-doped VWTi catalysts, which resulted from the promotional effect of ceria on the oxidation of NO to NO₂.^[10] Furthermore, the modification of V-SCR catalysts with iron oxide were as well reported to enhance the NO_x reduction activity.^[6b–e,g,11] The presence of cerium and iron could also be beneficial due to their known ability to oxidize volatile organic compounds (VOC) and soot.^[12] In this regard, the Ce⁴⁺/Ce³⁺ redox switch has often been exploited for oxidation reactions.^[13] Christensen *et al.*^[12a] demonstrated that ceria exhibits excellent soot oxidation activity due to the low oxygen bond strength. Ceria-based materials including doped ceria are also widely used for oxidation of hydrocarbons.^[12b] For example, Garcia *et al.*^[12c] reported that CeO₂ prepared by a precipitation method with urea was very active for naphthalene oxidation with 100% CO₂ selectivity even at 175 °C. Ceria-zirconia mixed oxides are as well applied due to their ability to oxidize different classes of volatile organic compounds (VOC) and soot, and actively support NH₃-SCR as component of various catalysts.^[14] Similarly, Fe-based catalysts are known to be active for CO, hydrocarbon and soot oxidation,^[12d–f,15] being attractive for 2-way SCR on DPF catalysts as well. Fe₂O₃-catalysts show excellent soot oxidation activity due to the transfer of surface and bulk oxygen from the catalyst to the surface of soot.^[12e,f] Finally, Waglöhner and Kureti reported that soot oxidation is almost fully selective to CO₂ over Fe₂O₃-catalysts, with an onset temperature of around 400 °C even for the catalyst-soot loose contact case.^[12f] This high

[a] L. Zheng, Dr. A. Zimina, Dr. M. Casapu, Prof. J.-D. Grunwaldt
Institute for Chemical Technology and Polymer Chemistry (ITCP)
Karlsruhe Institute of Technology (KIT)
Engesserstraße 20
76131 Karlsruhe (Germany)
E-mail: maria.casapu@kit.edu

[b] Dr. A. Zimina, Prof. J.-D. Grunwaldt
Institute of Catalysis Research and Technology (IKFT)
Karlsruhe Institute of Technology (KIT)
Hermann-von-Helmholtz-Platz 1
76344 Eggenstein-Leopoldshafen (Germany)

Supporting information for this article is available on the WWW under <https://doi.org/10.1002/cctc.202001314>

© 2020 The Authors. Published by Wiley-VCH GmbH. This is an open access article under the terms of the Creative Commons Attribution License, which permits use, distribution and reproduction in any medium, provided the original work is properly cited.

selectivity towards CO₂ is a promising aspect since the oxidation of VOC, such as C₃H₆, *o*-C₈H₁₀, *n*-C₁₂H₂₆, and of soot over typical vanadium-based SCR catalysts leads to significant amounts of CO emissions,^[16] demanding for further catalyst development.

In the present study, we systematically investigated the VOC and soot oxidation performance of Ce- and Fe-doped V₂O₅-WO₃/TiO₂ NO_x-SCR catalysts. They were studied in fresh state and after thermal aging, and compared to the activity of a typical VWTi catalyst. Propylene, *o*-xylene and *n*-dodecane were used as model VOCs for short chain, aromatic and long chain hydrocarbons, and carbon black to represent the diesel soot.

2. Results and Discussion

2.1. Catalyst characterization

The three catalyst series VWTi (3 wt% V₂O₅-10 wt% WO₃/TiO₂, cf. experimental section), and the 3 wt% Fe₂O₃- and 6 wt% CeO₂-doped catalysts (denoted VWTi-Fe and VWTi-Ce, respectively) were analyzed with respect to their chemical composition using inductively coupled plasma optical emission spectroscopy (ICP-OES). The elemental compositions were very close to the targeted compositions, as shown in Table S1. Hardly any change of the sample compositions was noticed after thermal aging treatment at 650 °C for 10 h for all three series of catalysts.

The specific surface area of selected samples is reported in Table 1. The results indicate that the BET surface area of the as prepared VWTi sample slightly decreases (from 64 to 52 m²/g) after the addition of cerium oxide but remains similar if iron oxide is included in the catalyst composition. Further thermal aging led to a stronger material sintering, particularly for the VWTi catalyst series. After calcination at 650 °C for 10 h, a surface area of only 9 m²/g was measured for VWTi-650, as compared with 19 and 21 m²/g for VWTi-Ce-650 and VWTi-Fe-650, respectively. The main reflection at 25.4° in the X-ray diffraction (XRD) pattern (Figure S1), typical for the anatase phase of TiO₂, was used to determine the crystallite sizes listed in Table 1. Higher thermal aging temperature resulted in a progressive growing of the crystallite size, with the larger sizes measured for VWTi-Fe-700 and VWTi-700 aged catalysts (65.3 nm and 77.3 nm, respectively). In contrast, the cerium-doped sample was less affected by the thermal aging treatment, with a crystallite size growth of only 5.2 nm after thermal aging at 700 °C for 10 h in comparison to the fresh state. This beneficial effect of cerium addition was as well observed when

using less or excess of cerium relative to vanadium loading in VWTi-Ce sample, as shown in Figure S2.

The total number of acidic sites evaluated based on the temperature-programmed desorption of ammonia (NH₃-TPD) results (Figure S3) and normalized versus fresh VWTi sample (Table 1) shows that the thermal aging treatment at high temperature diminished the number of acidic sites, particularly for the VWTi catalyst, which is known to be detrimental for the SCR performance.^[1b,17]

Raman spectroscopy was used to identify the different crystalline phases in the fresh and thermally aged catalysts. Selected Raman spectra are shown in Figure 1 in the range between 800 and 1200 cm⁻¹. Similar to the XRD results (Figure S1), the strong bands corresponding to the anatase TiO₂ phase were observed for all catalysts (Figure S4).^[18] The band at 858 cm⁻¹ recorded for VWTi-Ce-650 and VWTi-Ce-700 (Figure 1(b)) has been previously attributed to cerium vanadate.^[19] The formation of cerium vanadate in the 650 °C and 700 °C aged catalysts was also confirmed by XRD measurements (Figure S1). Moreover, iron vanadate was found in VWTi-Fe-600 and VWTi-Fe-650 catalysts (Figure 1(c)), as indicated by the band at 881 cm⁻¹.^[6f,20] Its disappearance upon thermal aging at 700 °C correlates to the decomposition of the iron vanadate phase, which has been suggested to start already at 600 °C by Marberger *et al.*^[6b,e] Hence, the formation as well as the decomposition of iron vanadate occurred at a lower temperature in comparison with cerium vanadate. Polymeric vanadates were reported as active species for the SCR reaction.^[1b] The presence of polymeric vanadates (V=O stretching vibrations) in all fresh catalysts was indicated by the Raman bands in the range of 940–990 cm⁻¹.^[21] For all three series of catalysts, the V=O stretching bands shifted to lower wavenumbers with higher thermal aging temperature, demonstrating the diminishment of the polymeric vanadates content. A more pronounced decrease was found for VWTi-650 and VWTi-700, as well as for VWTi-Fe-700. The appearance of rutile TiO₂ phase was also observed for these catalysts, as indicated by the bands at 808 cm⁻¹ (Figure 1(a)), 804 cm⁻¹ (Figure 1(c)) as well as 442 and 438 cm⁻¹ in Figure S4.^[22]

The UV-vis spectra of the investigated catalysts are shown in Figure 2. The absorption at wavelengths lower than 580 nm corresponds to the charge transfer signal of V⁵⁺ species (O²⁻ to V⁵⁺) and the absorption above 600 nm was attributed to the charge transfer from the d-orbital of V⁴⁺ to the conduction band of TiO₂.^[23] It has been reported that vanadium species interacting with titania boost the sintering of the TiO₂ support.^[1b] A more pronounced absorption in the region

Table 1. Structure characterization for selected samples.

Sample/T _{aging}	VWTi		VWTi-Ce		VWTi-Fe	
	fresh	650 °C	fresh	650 °C	fresh	650 °C
S _{BET} [m ² /g]	64	9	52	19	62	21
d [nm] ^[a]	17.0	63.2	18.3	21.3	17.4	23.5
Acidic sites ^[b]	1	0.18	0.84	0.51	0.98	0.47

[a] Crystallite size of titania estimated from XRD using the Scherer equation. [b] Relative total number of acidic sites normalized by that obtained for the VWTi fresh catalyst.

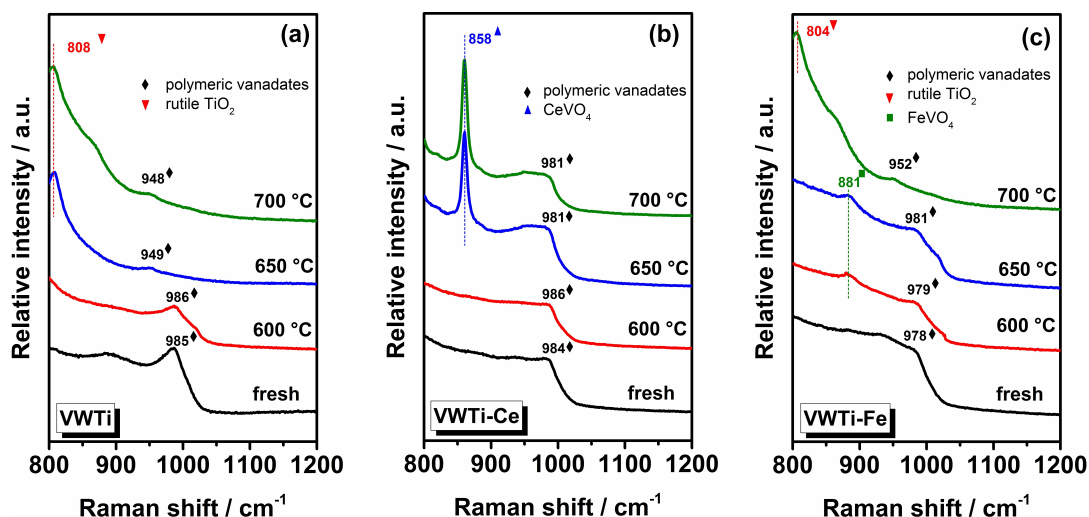


Figure 1. Raman spectra of investigated samples in the selected range of 800–1200 cm^{-1} (full Raman spectra, cf. Figure S4 in the Supporting Information): (a) VWTi, (b) VWTi–Ce and (c) VWTi–Fe fresh as well as 600 °C, 650 °C and 700 °C thermally aged catalysts.

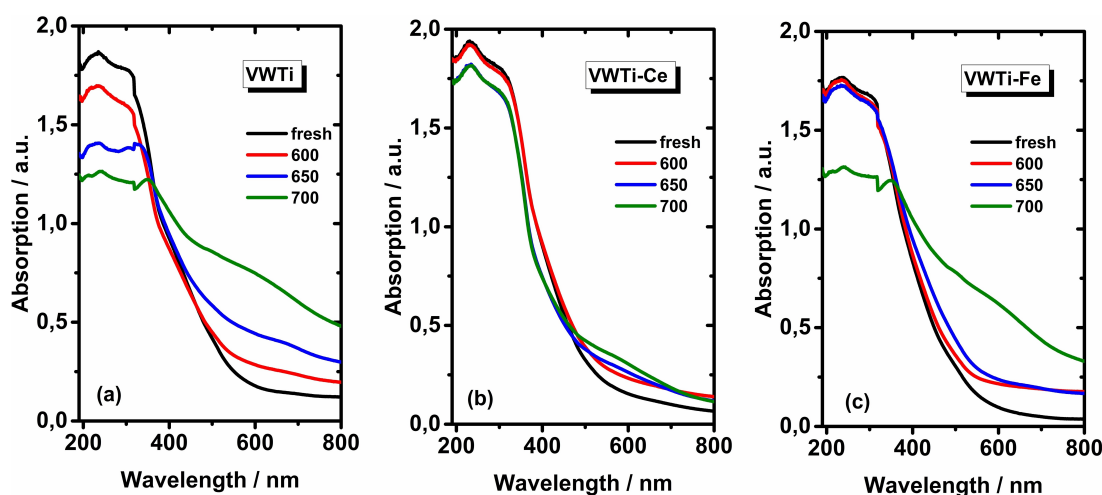


Figure 2. UV-vis spectra of (a) VWTi; (b) VWTi–Ce and (c) VWTi–Fe fresh as well as 600 °C, 650 °C and 700 °C thermally aged catalysts.

starting from 400 nm up to 800 nm was observed for the VWTi catalyst upon thermal aging, indicating more intimate V–Ti interaction.^[23] For Ce- and Fe-doped catalysts, only minor changes were measured during thermal aging process (except VWTi–Fe–700), and this can be explained by the weaker V–Ti interaction due to metal vanadates formation, as confirmed by the XRD (Figure S1) and Raman spectroscopy (Figure 1) results. Therefore, the moderate sintering process of the Ce- and Fe-doped catalysts during thermal aging could be explained by the formation of metal vanadates that weaken the V–Ti interaction thus retarding the sintering of the support.^[6b]

The profile of the temperature-programmed reduction with hydrogen (H_2 -TPR, Figure 3) recorded for the VWTi fresh catalyst shows a main peak at 424 °C and a shoulder at 539 °C, which were attributed to the reduction of highly dispersed vanadium species. The peak appearing at a higher temperature around 813 °C is due to the reduction of tungsten oxide.^[11] Upon CeO_2

addition, the reduction extent measured between 300–600 °C increases (maximum at 454 °C) due to overlap with the reduction of surface Ce^{4+} to Ce^{3+} in the same temperature region.^[10] This is confirmed by comparing the reduction profile of the VWTi–Ce catalyst with the results obtained for a V-free WTi–Ce sample as shown in Figure S5. The addition of Fe to the VWTi caused a lower onset temperature for reduction with the peak maximum at 400 °C and 752 °C, which is due to the simultaneous reduction of Fe_2O_3 .^[11,12d]

Upon thermal aging, the reduction peaks shifted to higher temperatures and became smaller for all catalyst series, suggesting a gradual decrease of catalyst reducibility. The new emerging peaks at 635 °C, 645 °C and 631 °C from VWTi–650, VWTi–700 and VWTi–Fe–700 catalysts, might be explained by the rutile TiO_2 formation, as anatase to rutile phase transformation were found for those catalysts (according to the XRD results in Figure S1 and Raman results in Figure 1). In addition,

the disappearance of the peak around 450–460 °C for cerium doped catalysts after thermal aging at 650 °C and 700 °C can be traced back to the formation of cerium vanadate. A similar tendency was observed for high cerium loaded catalysts, *i.e.* VWTi-2Ce, as shown in Figure S5(c). Pronounced variations in the TPR profile were recorded also for the VWTi-Fe samples due to formation of iron vanadate and catalyst sintering processes.

The formation of metal vanadates in Fe- and Ce-doped catalysts during thermal aging treatment was confirmed also by X-ray absorption spectroscopy (XAS) measurements. The normalized X-ray absorption near edge structure (XANES) spectra recorded at Ce L₃- and Fe K-edges for the Ce- and Fe-containing samples are shown in Figure 4(a) and (b), respectively. For the cerium containing samples, VWTi-Ce and VWTi-Ce-600, a similar XANES profile was observed as for the Ce⁴⁺ reference sample (CeO₂), due to the presence of CeO₂ in these catalysts

(*cf.* XRD data, Figure S1(b)). Major changes were noticed with higher thermal aging temperatures: the XANES spectra of VWTi-Ce-650 and VWTi-Ce-700 were very similar to the Ce³⁺ reference sample (ref. Ce(NO₃)₃), which also based on findings by Kumar *et al.*^[24] indicates the formation of CeVO₄. In addition to the variation in oxidation state, the formation of cerium vanadate involves the change of the crystal structure from cubic (CeO₂) to tetragonal. Furthermore, a slight increase of the Ce L₃-edge white line intensity was observed for the VWTi-Ce-700 sample in comparison to the catalyst calcined at 650 °C, probably due to the higher degree of crystallinity of the more strongly sintered catalyst. This evolution is supported by the corresponding XRD patterns (Figure S1).

For the Fe-doped catalysts, two characteristic features at 7114.8 and 7118.4 eV in the pre-edge region were clearly visible (Figure 4(b)), but did not appear for the Fe-reference samples (also indicated from Boubnov *et al.*^[25] for staurolite, FeO, FePO₄

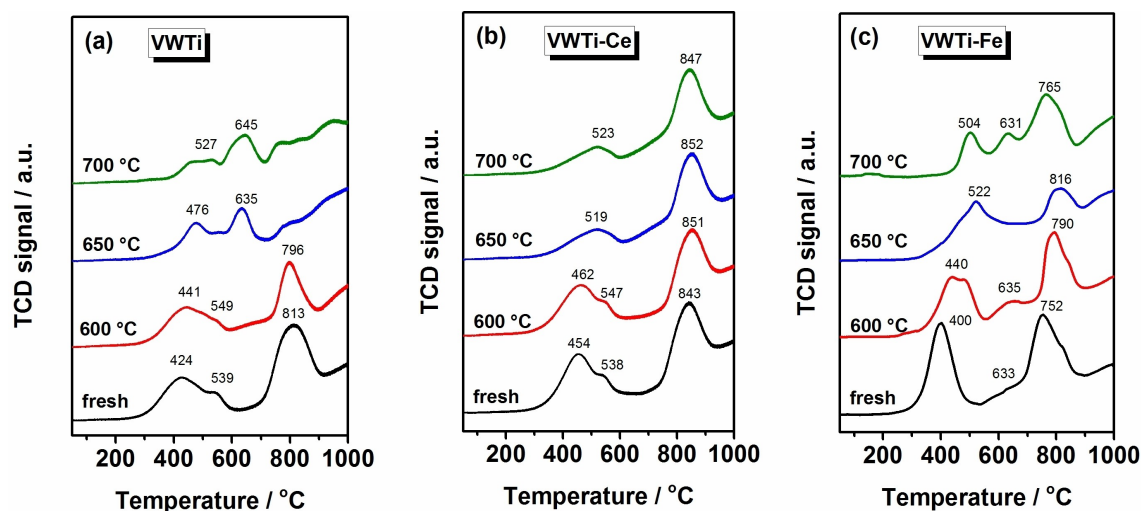


Figure 3. H₂-TPR results of the (a) VWTi; (b) VWTi-Ce and (c) VWTi-Fe fresh as well as 600 °C, 650 °C and 700 °C thermally aged catalysts.

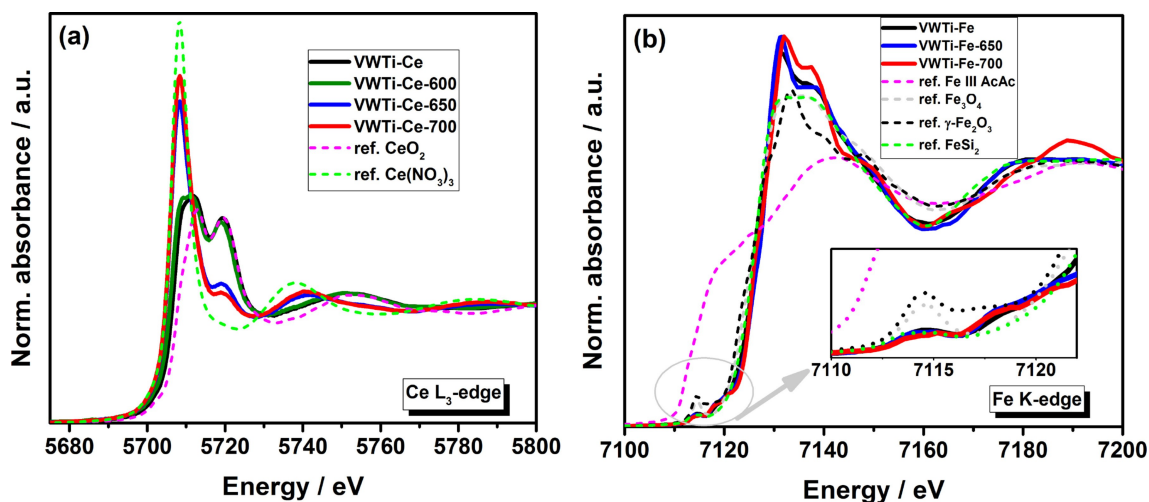


Figure 4. Normalized X-ray absorption near edge structure (XANES) spectra of (a) Ce L₃-edge of Ce-containing samples and (b) Fe K-edge of Fe-containing samples, as well as their corresponding reference sample.

reference samples). This region of the spectra resulting from $1s \rightarrow 3d$ (quadrupolar) and/or $1s \rightarrow 4p$ (dipolar) electronic transitions is mainly influenced by the oxidation state and coordination geometry of the Fe sites.^[25–26] According to previous studies,^[66,27] the two peaks can be attributed to surface FeVO_4 . This indicates that a strong interaction distorting the local geometry around the Fe atoms or the formation of FeVO_4 takes place already in the fresh VWTi–Fe sample. However, this change was not detected by Raman spectroscopy (Figure 1(c)) and XRD (Figure S1(c)) measurements, probably due to the presence of amorphous or short range ordered phases. Moreover, the XANES post-edge region of Fe-doped catalysts was completely different from that of reference samples, which represents another evidence for surface FeVO_4 formation.^[66] For the VWTi–Fe–700 sample the two features were still present in the XANES pre-edge region, indicating that FeVO_4 was not completely decomposed. Moreover, the more pronounced features in the XANES region could be related to a further particle size increase during catalyst calcination at 700°C . Unfortunately, due to the low loading and overlap with the TiO_2 rutile phase and WO_3 , the formation, sintering or decomposition of FeVO_4 could not be identified in the corresponding XRD patterns (Figure S1). The extended X-ray absorption fine structure (EXAFS) of VWTi–Fe fresh as well as 650°C and 700°C thermally aged samples was fitted using FeVO_4 as reference, and the results are presented in Figure S6 and Table S2. The rather high fitting degree again indicates the formation of FeVO_4 species in all investigated samples.

Based on the results obtained by the different complementary characterization methods including the sufficiently long thermal aging time, it can be concluded that most of vanadium species are present as CeVO_4 and FeVO_4 in the aged catalysts. However, we cannot completely exclude that a small amount of vanadium remains in the initial oxide state, namely V_2O_5 , and participates to the catalytic reactions as well.

2.2. SCR of NO_x with NH_3

The NH_3 –SCR performance of the fresh and thermally aged VWTi, VWTi–Ce and VWTi–Fe samples is presented in Figure 5. The as prepared VWTi shows a slightly broader temperature window for the SCR activity as compared with the Ce- and Fe-doped catalysts (a clearer comparison is provided in Figure S7). The VWTi–Ce and VWTi–Fe samples exhibit a NO_x conversion of 82.3% and 55.1% at 200°C , respectively. Both values are lower than 87.5%, as obtained for the VWTi catalyst for the same temperature point. This could be explained by the slightly decrease of the surface area and the total number of acidic sites (Table 1). Significant loss of activity was observed for the VWTi catalyst series with a NO_x conversion at 350°C of only 86.3% and 26.6% after thermal aging at 650°C and 700°C , respectively. On the contrary, apart from VWTi–Fe–700, the thermal aging treatment resulted in minor effects on the activity of Ce- and Fe-doped catalysts, for which full NO_x conversion maintained in the temperature range of 300 – 450°C . These results confirm the beneficial effect of adding cerium or iron oxide with respect to the thermal stability of vanadium-based SCR catalysts. This can be traced back to the formation of metal vanadates (Figures S1, 1 and 4), as it has been reported also by other groups.^[6b–e,11] However, FeVO_4 is less thermally stable and decomposes during aging at 700°C , leading to a severe deactivation of VWTi–Fe–700 catalyst, which shows the highest NO_x conversion of only 36% at 350°C . Hence, the structural evolution as uncovered in this study by Raman spectroscopy (Figure 1) and XAS (Figure 4) strongly correlates to the catalytic performance.

A similar beneficial effect on the thermal resistance was observed when using lower or higher cerium loadings relative to the vanadium content. For samples containing Ce:V molar ratios of 0.5 and 2, no major difference could be observed for the fresh and up to 650°C aged catalysts (Figure S8). However, the catalyst with a Ce:V ratios of 1 maintained the highest NO_x

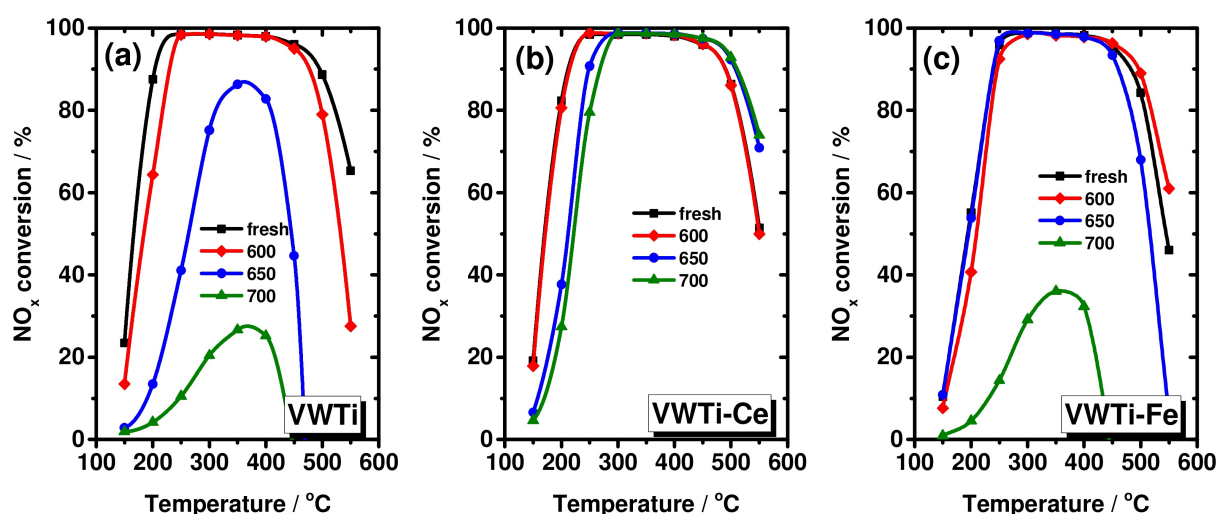


Figure 5. Catalytic performance under standard SCR condition: (a) VWTi; (b) VWTi–Ce and (c) VWTi–Fe fresh as well as 600°C , 650°C and 700°C thermally aged catalysts. 500 ppm NO , 500 ppm NH_3 , 5% H_2O , 10% O_2 in N_2 , GHSV = $50,000\text{ h}^{-1}$.

removal activity upon thermal aging at 700 °C for 10 h. 80% NO_x conversion during SCR at 250 °C was still observed for the VWTi–Ce-700 sample whereas only 53% and 61% were measured for VWTi-0.5Ce-700 and VWTi-2Ce-700 samples, respectively.

2.3. Hydrocarbon oxidation

The catalytic performance of the fresh and 650 °C thermally aged catalysts for propylene, *o*-xylene or *n*-dodecane oxidation in a gas mixture additionally containing 5% H₂O, 10% O₂ in N₂ is compared in Figure 6. Full conversion of propylene was obtained for all fresh catalysts starting with 400 °C whereas at lower temperature only *o*-xylene and *n*-dodecane were converted. This is in accordance with our previous study showing that hydrocarbons with longer chain length are more easily oxidized,^[16b] due to the fact that more adjacent sites are exposure for adsorption, as suggested by Yao *et al.*^[28] The results also indicate that for the fresh catalysts vanadium species act as active sites not only for NH₃–SCR reaction but also for hydrocarbon oxidation. The addition of Fe and Ce as dopants and the formation of metal vanadates leads to a slightly lower activity for hydrocarbon oxidation in comparison to the VWTi sample. This could be explained by a decreased availability of mobile oxygen. As the H₂-TPR results (Figure 3) revealed, the formation of vanadates and material sintering resulted in a higher reduction temperature and lower reduction extent as compared to the VWTi catalyst. However, the advantage of an increased thermal stability is clearly visible upon aging experiments. The oxidation activity drastically decreased for VWTi after calcination at 650 °C and only 70% propylene conversion was measured at 550 °C. For the same catalyst, the full conversion of *o*-xylene and *n*-dodecane shifted with 100 °C and 150 °C to higher temperature, respectively. This is due to the transformation of anatase to rutile upon high

temperature aging (as indicated by Raman results in Figure (1)), which is typically encountered for V–TiO₂ catalysts.^[16a,29] In contrast, for both doped samples only a minor diminishment of the oxidation activity was observed, particularly for the VWTi–Fe-650 catalyst. Therefore, due to the formation of metal vanadates upon thermal aging, Ce- and Fe-doped catalysts maintain not only their NH₃–SCR performance but also the hydrocarbon oxidation activity. In addition, improved CO₂ selectivity from hydrocarbon oxidation was also measured for VWTi–Ce and VWTi–Fe catalysts. Similarly as observed for the NO_x removal activity, the rate of the hydrocarbon oxidation was kept high for catalysts with different cerium loadings (Figure S9), an intermediate cerium loading (V/Ce = 1) still resulting in the highest activity in spite of the high thermal aging temperatures. In all cases, CO and CO₂ were detected as major products, accompanied by small amounts of oxygenates, such as formaldehyde at intermediate temperatures. The occurring processes will be discussed in more detail in the following sections.

2.4. SCR of NO_x with NH₃ in the presence of hydrocarbons

NH₃–SCR performance in the presence of hydrocarbons (propylene, *o*-xylene and *n*-dodecane) was evaluated for the fresh (Figure 7) and 650 °C thermally aged catalysts (Figure 8). All three hydrocarbons slightly inhibited the NO_x removal activity in the high temperature region due to the competition for active sites, since both hydrocarbon oxidation and NH₃–SCR require the vanadium species for adsorption and activation.^[16a,b] However, the short and long chain hydrocarbons display different NH₃–SCR inhibition tendency at low temperatures. Similarly as observed in our previous study,^[16b] *n*-dodecane, which is easier to oxidize (Figure 6), shows a stronger *n*-inhibition effect in comparison to short chain hydrocarbons. As displayed in Figure 7, for the fresh catalysts, hardly any influence of

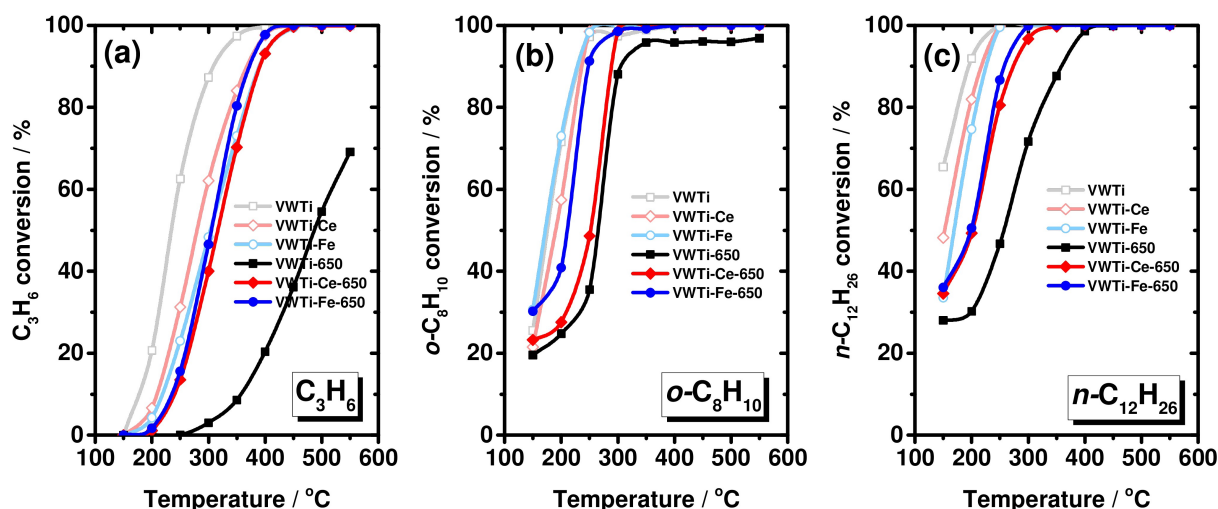


Figure 6. Hydrocarbon oxidation over fresh and 650 °C thermally aged VWTi, VWTi–Ce and VWTi–Fe catalysts: (a) propylene conversion; (b) *o*-xylene conversion and (c) *n*-dodecane conversion. 185 ppm C₃H₆ (or 80 ppm *o*-C₈H₁₀ or 80 ppm *n*-C₁₂H₂₆), 5% H₂O and 10% O₂ in N₂, GHSV = 50,000 h⁻¹.

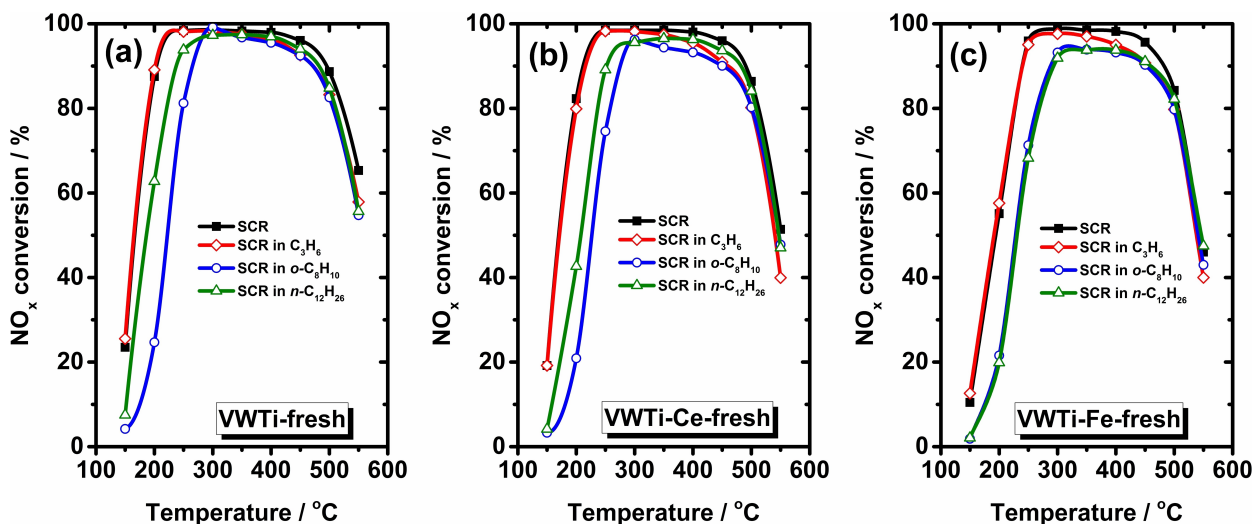


Figure 7. NH_3 -SCR performance in presence of hydrocarbons (propylene, *o*-xylene and *n*-dodecane) over fresh catalysts: (a) VWTi; (b) VWTi-Ce and (c) VWTi-Fe. 500 ppm NO , 500 ppm NH_3 , (185 ppm C_3H_6 , 80 ppm *o*- C_8H_{10} or 80 ppm *n*- $\text{C}_{12}\text{H}_{26}$ dosed optionally), 5% H_2O , 10% O_2 in N_2 , GHSV = 50,000 h^{-1} .

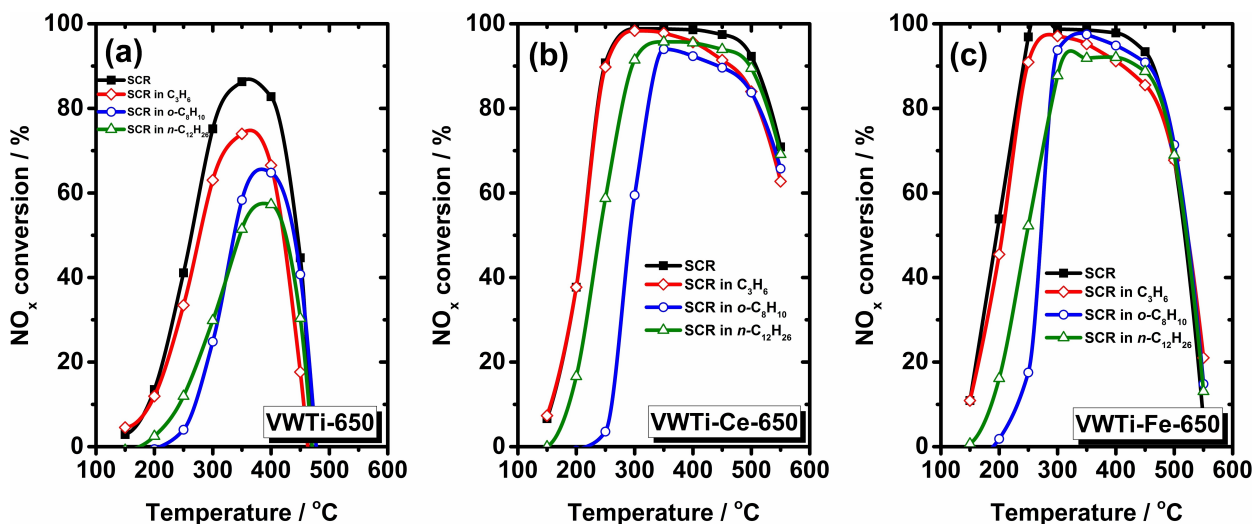


Figure 8. NH_3 -SCR performance in presence of hydrocarbons (propylene, *o*-xylene and *n*-dodecane) over 650°C thermally aged catalysts: (a) VWTi-650; (b) VWTi-Ce-650 and (c) VWTi-Fe-650. 500 ppm NO , 500 ppm NH_3 (185 ppm C_3H_6 , 80 ppm *o*- C_8H_{10} or 80 ppm *n*- $\text{C}_{12}\text{H}_{26}$ dosed optionally), 5% H_2O , 10% O_2 in N_2 , GHSV = 50,000 h^{-1} .

propylene was noticed, which is in accordance with previous studies,^[16a,b,30] while a clear inhibition effect was observed for *n*-dodecane. Analogously, *o*-xylene shows an inhibition effect on NO_x conversion that is more pronounced in comparison to *n*-dodecane, particularly for VWTi and Ce-doped catalysts. For the VWTi catalyst, the NO_x conversion of 89.1% at 200°C decreased to 62.7% in the presence of *n*-dodecane and to 24.7% if *o*-xylene was added. As for VWTi-Ce, the 79.9% NO_x conversion at 200°C decreased to 42.7% or 20.9% in a gas mixture containing *n*-dodecane or *o*-xylene, respectively. In contrast, for VWTi-Fe the inhibition effect of *n*-dodecane and *o*-xylene is similar, both decreased the NO_x removal activity from 55.1% conversion to 19.8% at 200°C.

After thermal aging at 650°C (Figure 8), a similar trend was observed as for the fresh catalyst. In the presence of *n*-dodecane a conversion drop of ca. 30% was found at 250°C for both VWTi-650 and VWTi-Ce-650 catalysts. *o*-Xylene addition led to an even more severe decrease, from 41.1% conversion at 250°C to 4.0% for VWTi-650 and from 90.7% to 3.6% for VWTi-Ce-650. For VWTi-Fe-650, the NO_x conversion at 250°C is with 45% and 79% lower in the presence of *n*-dodecane and *o*-xylene, respectively. As illustrated in Figure 8, even after the thermal aging treatment at 650°C for 10 h, the Ce- and Fe-doped catalysts exhibited higher NO_x removal activity in presence of hydrocarbons as compared with VWTi. An analogous effect of propylene presence on the SCR activity, *i.e.* only slightly inhibited the NO_x removal activity in the high temper-

ature region, was observed for catalysts containing different cerium loadings (results not shown). This is partially due to the known SCR activity of Ce-based SCR catalysts,^[31] as measured also in the present study for a V-free WTi-2Ce catalyst (Figure S8(a)). A complementary estimation of the effect of different hydrocarbons at intermediate temperatures (250 - 400 °C) could be conducted by using a lower catalyst load for the NH₃-SCR activity tests, to prevent close to full conversion for all investigated samples.

2.5. Hydrocarbon oxidation in presence of standard SCR conditions

The hydrocarbon oxidation performance, with and without the presence of the standard SCR conditions was systematically compared over fresh (Figure S10) and 650 °C thermally aged catalysts (Figure S11). In general, the standard SCR gas mixture did not significantly influence the hydrocarbon conversion, and a more pronounced inhibition effect was observed only at low temperatures. The corresponding T_{50} (temperature of 50% conversion) temperatures are plotted in Figure 9. In all cases, the T_{50} for hydrocarbon oxidation shifted to higher temperature under SCR conditions. The highest shift of about 60 °C was measured for VWTi during *n*-dodecane oxidation. More importantly, after the thermal treatment at 650 °C for 10 h, the Ce- and Fe-doped catalysts exhibited lower T_{50} temperatures in comparison to the VWTi-650 sample. This clearly indicates that the addition of Ce and Fe dopants helps in stabilizing not only the SCR performance but also the hydrocarbon oxidation activity (Figure 5, Figure 6, Figure S8), which is highly relevant for 2-way SCR on DPF applications.

The CO₂ and CO emissions resulting from the hydrocarbon oxidation, with (*i.e.* 500 ppm NO, 500 ppm NH₃) and without (*i.e.* no NO/NH₃ in the feed) the presence of standard SCR

conditions, over the fresh catalysts are shown in Figure S12 and Figure S13, respectively. The rather complex CO and CO₂ concentration profiles suggest different reaction mechanisms and reaction intermediates as the temperature increases. According to Koebel and Elsener,^[16c] monocarboxylic and dicarboxylic acids are formed from VOC oxidation at low temperature, by their decomposition leading to CO formation as the temperature increases. Additionally, the adsorption, desorption and later oxidation of such reaction intermediates might also contribute to the uneven CO and CO₂ emission profiles. The CO₂ selectivity, in terms of $[\text{CO}_2]/([\text{CO}] + [\text{CO}_2])$ ratio, over fresh and 650 °C aged samples is shown in Figure 10 and Figure S14, respectively. For all fresh catalysts the CO₂ selectivity was in the range of 20–40% during propylene oxidation, and high CO concentrations were simultaneously detected. A higher CO₂ selectivity was found during *o*-xylene and *n*-dodecane oxidation, amounting to 60–90% and 40–90%, respectively. The addition of cerium or iron to the VWTi catalyst has only a small beneficial effect on the CO₂ selectivity. Even higher CeO₂ loadings do not result in increased CO₂ emissions (Figure S15). This behavior is in contrast to the well-known ability of ceria and iron oxides-based catalysts to completely oxidize VOC and CO especially at high temperatures.^[12c,d,f] Probably, the strong interaction with vanadium leading to vanadates formation results in less redox active species (Figure 3). Nevertheless, the slight improvement towards the desired product CO₂, as shown by the vanadate-based catalysts, combined with their superior thermal stability represents an advantage for a potential multifunctional catalyst.

Obviously, the presence of the standard SCR gas mixture promoted the CO₂ formation in the investigated temperature range, regardless of catalyst composition, aging state and hydrocarbon structure. This promoting effect is probably due to the presence of NO_x (particularly NO₂ formation via NO oxidation) and the resulting more oxidative environment.

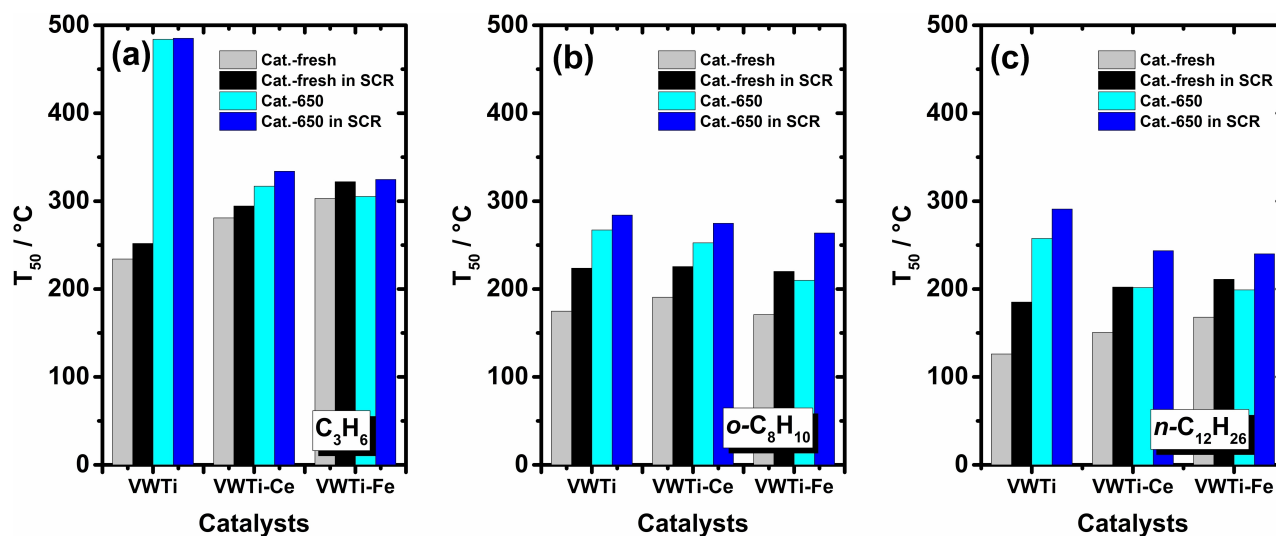


Figure 9. Comparison of T_{50} temperatures for hydrocarbon oxidation with and without the presence of standard SCR condition over investigated fresh as well as 650 °C thermally aged catalysts: (a) propylene oxidation (b) *o*-xylene oxidation and (c) *n*-dodecane oxidation. 185 ppm C₃H₆ (or 80 ppm *o*-C₈H₁₀ or 80 ppm *n*-C₁₂H₂₆), (500 ppm NO, 500 ppm NH₃, when in presence of standard SCR), 5% H₂O and 10% O₂ in N₂, GHSV = 50,000 h⁻¹.

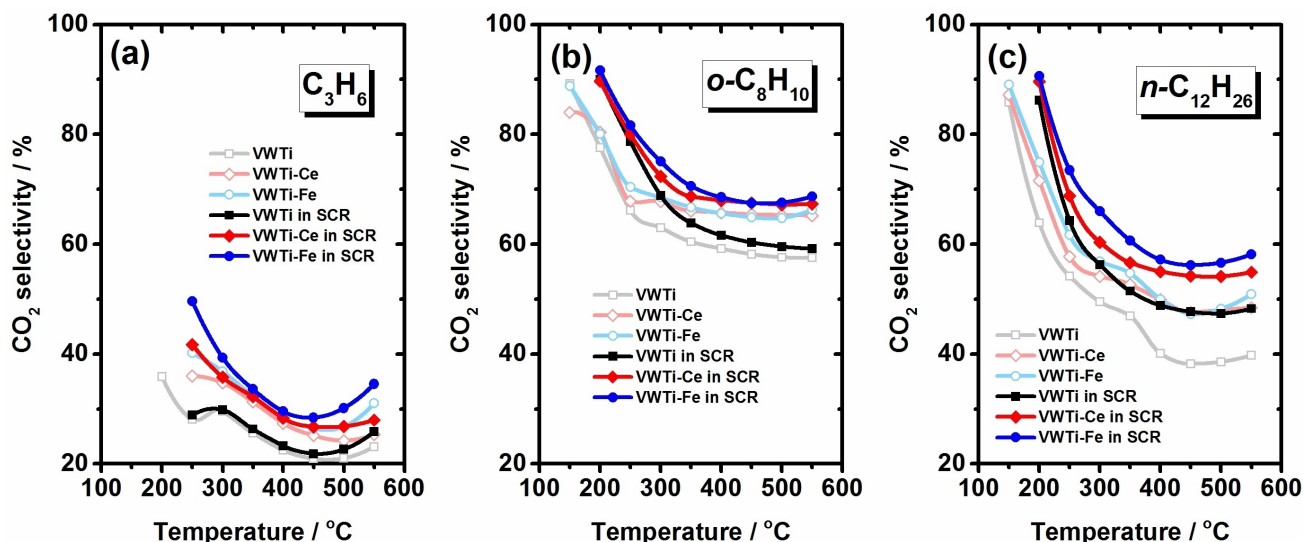


Figure 10. Comparison of CO₂ selectivity during hydrocarbon oxidation with and without the presence of standard SCR condition over 3VWTi, Ce- and Fe-doped 3VWTi fresh catalysts: (a) propylene oxidation; (b) *o*-xylene oxidation and (c) *n*-dodecane oxidation. 185 ppm C₃H₆ (or 80 ppm *o*-C₈H₁₀ or 80 ppm *n*-C₁₂H₂₆), (500 ppm NO, 500 ppm NH₃, when in presence of standard SCR), 5% H₂O and 10% O₂ in N₂, GHSV = 50,000 h⁻¹.

However, the CO₂ selectivity decreases with temperature (Figure 10 and S14) indicating that the partial oxidation instead of total oxidation is favored. As mentioned above, this could be due to a switch in the reaction mechanism. At the same time, such a behavior might be caused by the inhibition of catalyst reoxidation due to the presence of NH₃, CO and other carbonaceous species.^[2a]

2.6. Soot oxidation

In addition to hydrocarbon oxidation, soot oxidation was evaluated and the corresponding CO and CO₂ emissions are plotted in Figure 11. As shown in Figure 11(a), when the pure soot is heated up in inert atmosphere (N₂), only a slight oxidation was detected above 200 °C, with two maxima at

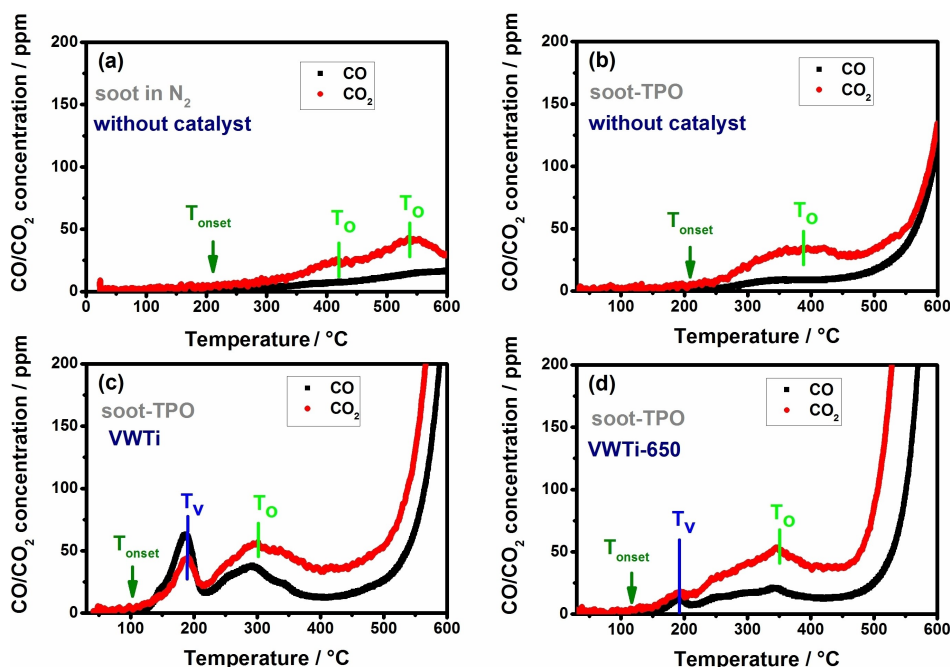


Figure 11. Comparison of CO and CO₂ emissions from soot oxidation: (a) pure soot heating up in N₂ without catalyst; (b) soot-TPO without catalyst; (c) soot-TPO with VWTi; (d) soot TPO with VWTi-650. 100 mL/min N₂ (a) or 10% O₂/N₂ (b–d) with a temperature ramp of 10 °C/min to 600 °C. Marked temperatures represent: T_{onset} = temperature of soot oxidation onset; T_o = temperature maximum of the oxidation peak involving O-species; T_v = temperature maximum of the oxidation peak involving catalyst surface V-species.

409 °C and 545 °C (marked as T_O , oxidation by O-species), which was ascribed to oxidation by traces of oxygen or water present in the soot sample, as the O and OH radicals were reported to participate in the soot oxidation process.^[32] This temperature range corresponds to the oxidation of soot surface species or of smaller particles.^[33] Upon oxygen dosage (Figure 11(b)), the soot conversion significantly increased. This is due to the transfer of gaseous oxygen to the surface of soot,^[34] as shown from the shift and intensity of the T_O peaks. Additionally, another pronounced soot oxidation temperature range appeared above 500 °C, in line with literature data on the total oxidation of carbon black in the absence of a catalyst.^[35]

During soot oxidation in the presence of the fresh VWTi catalyst (Figure 11(c)), the onset temperature (T_{onset}) decreased to 102 °C accompanied by an increase of the intensity for T_O region. In addition, a new peak at 187 °C (marked as T_V , oxidation from V-species) was noticed and could be attributed to the soot oxidation via the contribution of VO_x species. This is in accordance with literature reports claiming that vanadium-based SCR catalysts are active for soot oxidation,^[16a,36] and the activity was found to correlate with the low oxygen bond strength of vanadia.^[12a] Moreover, the contact between soot and catalyst is a key factor for soot oxidation at low temperature.^[37] In this regard, the high mobility of V species in this temperature range (V_2O_5 with Tamman temperature of ~200 °C) leads to migration of the active phase, thus, improving the contact with the soot.^[38] In comparison to the fresh VWTi catalyst, the T_{onset} and T_O of VWTi-650 shifted to higher temperature with a sharp decrease also of T_V intensity. This behavior could be attributed to the decreased mobility of vanadium due to catalyst sintering (Table 1). However, the soot oxidation performance in the temperature range of 500–600 °C significantly improved for the thermally aged catalyst, and will be discussed in detail in the following part.

The fresh and 650 °C thermally aged Ce- and Fe-doped catalysts were also evaluated for the catalytic soot oxidation (Figure S16), the onset temperature as well as the temperature for the T_V peak are summarized in Figure 12(a). In general, over the doped catalysts the soot oxidation is shifted to higher temperatures. We assigned this inhibition effect to the decreased vanadium mobility because of metal vanadates formation, as demonstrated by the XRD (Figure S1), Raman spectroscopy (Figure 1) and XAS (Figure 4) results.

An overview on the soot oxidation performance around 600 °C of the different catalysts investigated in this study is reported in Figure 12(b). For all catalysts, the CO_2 emissions were higher than CO emissions. A CO_2 selectivity (in terms of $CO_2/(CO+CO_2)$ ratio) higher than 60% was measured for all samples, while VWTi-650 and VWTi-Fe-650 exhibited 82% and 80.5% selectivity, respectively. These two catalysts showed also the highest soot conversion at this temperature. For VWTi-650, the formation of larger V_2O_5 particles due to catalyst sintering seems to promote soot oxidation above 450 °C. In the case of VWTi-Fe-650, this behavior could be explained by the partial decomposition of $FeVO_4$ with V_2O_5 formation and catalyst sintering already at this moderate aging temperature, as shown by our characterization data (Figures 1, 4 and S1) and in line

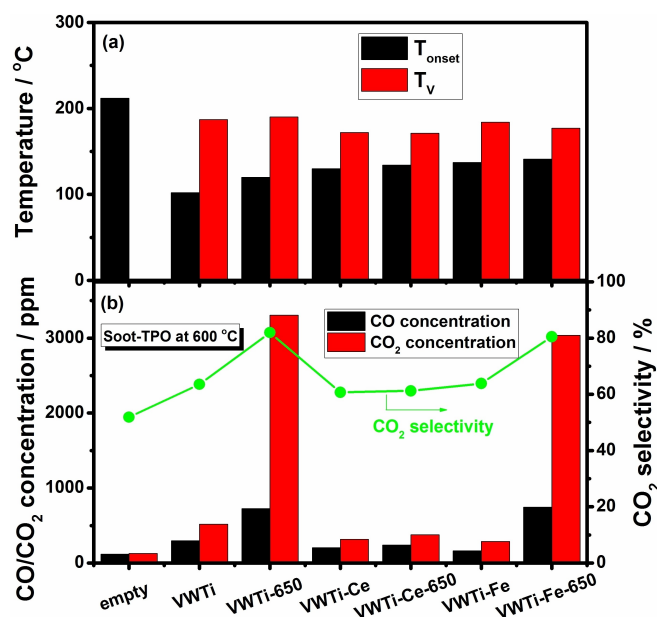


Figure 12. Soot oxidation without and with the presence of different catalysts: (a) comparison of the temperature for T_{onset} and T_V ; (b) comparison of the total CO, CO_2 emissions and CO_2 selectivity. Soot oxidation experiments were carried out in 10% O_2/N_2 , 100 mL/min, with a temperature ramp of 10 °C/min to 600 °C.

with Marberger *et al.*^[6b,e] According to previous studies, the extent of catalyst surface-soot particles contact represents a critical factor that determines the catalytic soot oxidation performance, particularly in the case of loose contact.^[38b] It has been suggested that only the outer surface of the catalyst contributes to the solid-solid contact.^[38b] Hence, catalysts with lower surface area might expose relatively more active sites for soot contact in comparison to high surface area catalysts, since the active sites inside pores are not accessible for soot oxidation. Liu *et al.*^[38b] reported that the low surface area V/ZrO_2 and V/TiO_2 catalysts are more active for soot oxidation in comparison to V/Al_2O_3 and V/SiO_2 with higher surface area. Accordingly, the very low specific surface area of 9 and 21 m^2/g observed for VWTi-650 and VWTi-Fe-650, respectively could partially explain their higher soot oxidation performance. However, even with a low surface area of 19 m^2/g , the VWTi-Ce-650 catalyst shows a lower soot oxidation activity as compared to VWTi-650 and VWTi-Fe-650. Hence, the presence of mobile V_2O_5 seems to have a higher impact, as free vanadium species were found to be highly active for soot oxidation.^[38b] The lower redox activity of cerium vanadates (according to the H_2 -TPR results, Figure 3(b)), that are still present in the VWTi-Ce-650 limits the soot oxidation activity of this catalyst. Regarding the soot oxidation mechanism at high temperature, since VWTi and VWTi-650 exhibit comparably low CO oxidation activity at 500–600 °C (Figure S17), the possibility that the high CO_2 selectivity of VWTi-650 is due to CO formed from soot oxidation which further oxidizes to CO_2 on the catalyst surface can thus be ruled out. Hence, VWTi-650 and VWTi-Fe-650 catalysts possibly produce more di-oxygenated carbon inter-

mediate species than mono-oxygenated surface species, finally resulting in more CO₂ desorption.^[39]

3. Conclusions

In the present study the catalytic performance of hydrocarbon (propylene, *o*-xylene and *n*-dodecane) and soot oxidation were systematically evaluated for Ce- and Fe-doped V₂O₅–WO₃/TiO₂ fresh and thermally aged catalysts, as potential systems for 2-way SCR on DPF applications. For the fresh catalysts only a minor decrease of both NH₃–SCR and hydrocarbon oxidation activity was observed as a result of Ce and Fe addition. This can be traced back to the slightly lower surface area and total number of acidic sites. In line with previous studies, the formation of metal-vanadates upon thermal aging, was demonstrated by XRD, Raman spectroscopy and *ex-situ* XAS measurements. A higher stability was found for CeVO₄ in comparison with FeVO₄.

In contrast to the conventional VWTi catalysts, Ce- and Fe-doped samples maintain not only a relatively good NH₃–SCR performance but also the hydrocarbon oxidation activity upon thermal aging at 700 °C and 650 °C, respectively. As indicated by spectroscopic investigations, this behavior could be explained by the formation of metal vanadates that weaken the V–Ti interaction and thus retard the support from severe sintering. Furthermore, the addition of the cerium or iron slightly promotes CO₂ formation in the investigated temperature range, regardless of hydrocarbon structure and catalyst aging state. The presence of the standard SCR gas mixture additionally enhanced the CO₂ selectivity, which was assigned to the presence of a more oxidative atmosphere. Finally, the doped catalysts are also attractive for catalyzing soot oxidation. In contrast to the NH₃–SCR and HC oxidation where highly dispersed V-species were identified as active sites, the presence of mobile V₂O₅ seems to be the driving parameter for a high activity and CO₂ selectivity. In spite of suffering from SCR and hydrocarbon oxidation activity loss, the sintering of the samples upon thermal aging, generates more catalyst-soot external surface contact points and also V₂O₅ mobile species, which significantly improve the soot conversion and CO₂ selectivity, as observed particularly for VWTi-650 and VWTi–Fe-650 catalysts.

In summary, the improved hydrothermal stability of the Ce- and Fe-doped catalysts in comparison to the conventional VWTi combined with good hydrocarbon and soot oxidation activity makes them promising candidates for combined SCR and DPF systems. Moreover, the slightly higher CO₂ selectivity measured during long or short chain hydrocarbon oxidation represents a notable advantage for a possible multifunctional catalyst. However, to further improve their performance and stability, fine tuning of the catalyst composition as well as combination of different dopants need to be considered in the future. Furthermore, for a final assessment compared to real applications, SO₂ poisoning tests should be conducted for all relevant reactions occurring on such multifunctional catalytic systems.

Experimental Section

Catalyst preparation

The vanadium-based SCR catalyst with a composition of 3 wt% V₂O₅–10 wt% WO₃/TiO₂ (VWTi) was prepared by incipient wetness impregnation. A commercial W/TiO₂ support (CristalACTIV™ DT-52, 10 wt% WO₃/TiO₂) was used and calcined in static air at 450 °C for 4 h prior to impregnation. Next, the ammonium metavanadate (Sigma) was dissolved in deionized water with the addition of oxalic acid (Merck) and the obtained solution was impregnated on the W/TiO₂ support. The sample was dried and then calcined at 550 °C for 4 h (defined as the fresh state).

Ce- and Fe-doped V–SCR catalysts with a V/dopant molar ratio of 1:1 were prepared by impregnation of cerium (III) nitrate hexahydrate (Alfa Aesar) or iron (III) nitrate nonahydrate (Alfa Aesar) aqueous solution on a fresh VWTi catalyst, respectively. The obtained samples were dried and then calcined at 550 °C for 4 h (defined as the fresh state). For inducing the formation of vanadates as well as for thermal stability tests, the prepared catalysts were further aged at different temperatures, *i.e.*, 600 °C, 650 °C and 700 °C for 10 h in static air. In the present study, the obtained samples will be referred as *e.g.* VWTi–Ce-600 for Ce-doped VWTi catalyst after thermal aging treatment at 600 °C for 10 h, VWTi–Fe-650 for Fe-doped VWTi catalyst after thermal aging at 650 °C for 10 h.

In order to investigate the impact of different V/Ce molar ratios on the SCR and hydrocarbon oxidation activity, additional samples were prepared with molar ratios of 0/1, 1/0.5 and 1/2 (WTi–Ce, VWTi-0.5Ce and VWTi-2Ce, respectively) in a similar way as mentioned above. The resulting catalysts were as well aged by a 10 h thermal treatment at 600 °C, 650 °C and 700 °C and used for tests on C₃H₆ oxidation in the presence or absence of the SCR gas mixture.

Characterization

The specific surface area of the prepared samples was measured by N₂ physisorption at –196 °C using multipoint measurements on a BELSORP-mini instrument (MicrotracBEL, Osaka, Japan). Prior to the measurement, all samples were degassed in vacuum at 300 °C for 2 h.

Raman spectroscopy measurements were conducted on a Renishaw inVia confocal Raman microscope. A Nd-YAG laser with a wavelength of 532 nm (100 mW) and a 2400 l/mm grating was used. Spectra were taken with 0.5% laser power and *ca.* 40–50 spectra of a small line area were measured which were averaged after cosmic ray removal using Renishaw WiRE™ software.

UV-vis spectra of the samples were recorded with a Lambda 650 instrument (PerkinElmer). Each spectrum was recorded from 190 to 800 nm with a scan speed of 0.5 s/nm.

Temperature programmed reduction with hydrogen (H₂-TPR) was performed using a Micromeritics AutoChem II 2920 chemisorption analyzer equipped with a thermal conductivity detector (TCD). Catalyst sample placed in U-shaped quartz tube was pretreated at 500 °C (10 °C/min) with 50 mL/min of 20.5% O₂/N₂. The sample was flushed with 50 mL/min Ar at 50 °C for 30 min followed by the TPR in the temperature range of 50 to 1000 °C in 50 mL/min of 10% H₂/Ar (10 °C/min).

X-ray absorption spectroscopy (XAS) measurements of cerium and iron doped samples were performed at the CAT-ACT beamline (KIT synchrotron, Karlsruhe)^[40] at Ce L₃-edge (5723 eV) and at the SUL–X

beamline (KIT synchrotron, Karlsruhe)^[41] at Fe K-edge (7112 eV), respectively. X-ray absorption spectra of the samples were recorded in transmission mode for the cerium doped samples and in fluorescence mode for the iron doped samples. In addition to the prepared catalyst samples, several reference samples were also recorded for comparison. The resulting XAS spectra were normalized using the ATHENA program from the IFFEFIT package.^[42]

The chemical composition of the fresh and 650 °C thermally aged catalysts was determined using inductively coupled plasma optical emission spectroscopy (ICP-OES) on an OPTIMA 4300 DV spectrometer (PerkinElmer).

The prepared samples were also characterized by X-ray diffraction (XRD) and temperature programmed desorption of ammonia (NH₃-TPD), a detailed description of the procedures is available in the SI.

Catalytic tests

All catalytic performance tests were carried out at steady-state condition in a quartz tube plug flow reactor (ID=8 mm). Gases were dosed individually by mass flow controllers (Bronkhorst) and the resulting gas stream was preheated to 150 °C before entering the quartz reactor. The gas composition after the reactor was analyzed with a MultiGas™ 2030 FTIR gas analyzer (MKS). For the standard SCR and hydrocarbon oxidation tests, the catalyst powder (500 mg, 125–250 μm) was mixed with quartz sand (500 mg, 125–250 μm) to reach a total bed length of 20 mm. The gas mixture for standard SCR was 500 ppm NO, 500 ppm NH₃, 5% H₂O, 10% O₂ in N₂ with a gas hourly space velocity (GHSV) of 50,000 h⁻¹. Propylene, *o*-xylene and *n*-dodecane were used as model hydrocarbons and their concentrations were: 185 ppm C₃H₆, 80 ppm *o*-C₈H₁₀ and 80 ppm *n*-C₁₂H₂₆ in 5% H₂O, 10% O₂ and balance N₂ at a GHSV of 50,000 h⁻¹. A homemade saturator with N₂ as carrier gas was used for the dosage of *o*-xylene and *n*-dodecane.

For the soot oxidation tests, the soot (20 mg, carbon black from Alfa Aesar) and the catalyst (80 mg, 125–250 μm) samples were mixed together with a spatula, resulting in a loose contact.^[12a,43] The reactor was heated up to 600 °C in 10% O₂/N₂ (100 mL/min) with a temperature ramp of 10 °C/min.

Acknowledgements

The authors gratefully acknowledge financial support of this work via provision of a PhD scholarship to L. Zheng by China Scholarship Council (CSC). We thank Jan Pesek for technical support with respect to catalysts testing. A. Deutsch (ITCP, KIT) is acknowledged for the BET measurements. Dr. T. Bergfeldt (IAM, KIT) is acknowledged for elemental analysis. We would like to thank the Institute for Beam Physics and Technology (IBPT) for the operation of the storage ring, the Karlsruhe Research Accelerator (KARA) and acknowledge in particular Dr. Tim Prüßmann (IKFT, KIT) for his help and technical support during experiments. We gratefully acknowledge KIT and Deutsche Forschungsgemeinschaft (DFG) for financing the Renishaw inVia Reflex Spectrometer System (INST 121384/73-1). Open access funding enabled and organized by Projekt DEAL.

Conflict of Interest

The authors declare no conflict of interest.

Keywords: vanadium · vanadates · SCR · hydrocarbon oxidation · soot oxidation

- [1] a) O. Deutschmann, J.-D. Grunwaldt, *Chem. Ing. Tech.* **2013**, *85*, 595–617; b) G. Busca, L. Lietti, G. Ramis, F. Berti, *Appl. Catal. B* **1998**, *18*, 1–36; c) L. Han, S. Cai, M. Gao, J. Hasegawa, P. Wang, J. Zhang, L. Shi, D. Zhang, *Chem. Rev.* **2019**, *119*, 10916–10976.
- [2] a) D. E. Doronkin, F. Benzi, L. Zheng, D. Sharapa, L. Amidani, F. Studt, P. W. Roesky, M. Casapu, O. Deutschmann, J.-D. Grunwaldt, *J. Phys. Chem. C* **2019**, *123*, 14338–14349; b) A. Marberger, D. Ferri, M. Elsener, O. Kröcher, *Angew. Chem. Int. Ed.* **2016**, *55*, 11989–11994; *Angew. Chem.* **2016**, *128*, 12168–12173; c) I. Nova, C. Ciardelli, E. Tronconi, D. Chatterjee, M. Weibel, *AIChE J.* **2009**, *55*, 1514–1529; d) N. R. Jaegers, J. K. Lai, Y. He, E. Walter, D. A. Dixon, M. Vasilii, Y. Chen, C. Wang, M. Y. Hu, K. T. Mueller, *Angew. Chem.* **2019**, *58*, 12739–12746.
- [3] M. T. Yan, S. Kureti, K. Hizbullah, N. Jan, *Chem. Eng. Technol.* **2007**, *30*, 1440–1444.
- [4] D. M. Chapman, *Appl. Catal. A* **2011**, *392*, 143–150.
- [5] P. Granger, H. W. Siaka, S. B. Umbarkar, *Chem. Rec.* **2019**, *19*, 1813–1828.
- [6] a) M. A. L. Vargas, M. Casanova, A. Trovarelli, G. Busca, *Appl. Catal. B* **2007**, *75*, 303–311; b) A. Marberger, D. Ferri, M. Elsener, A. Sagar, C. Artner, K. Schermanz, O. Kröcher, *Appl. Catal. B* **2017**, *218*, 731–742; c) M. Casanova, A. Sagar, K. Schermanz, A. Trovarelli, *Top. Catal.* **2016**, *59*, 996–1001; d) G. Wu, J. Li, Z. Fang, L. Lan, R. Wang, M. Gong, Y. Chen, *Catal. Commun.* **2015**, *64*, 75–79; e) A. Marberger, M. Elsener, D. Ferri, A. Sagar, K. Schermanz, O. Kröcher, *ACS Catal.* **2015**, *5*, 4180–4188; f) F. Liu, H. He, Z. Lian, W. Shan, L. Xie, K. Asakura, W. Yang, H. Deng, *J. Catal.* **2013**, *307*, 340–351; g) M. Casanova, J. Llorca, A. Sagar, K. Schermanz, A. Trovarelli, *Catal. Today* **2015**, *241*, 159–168.
- [7] a) X. Zhao, L. Huang, H. Li, H. Hu, X. Hu, L. Shi, D. Zhang, *Appl. Catal. B* **2016**, *183*, 269–281; b) A. Sagar, A. Trovarelli, M. Casanova, K. Schermanz, *SAE Int. J. Engines* **2011**, *4*, 1839–1849; c) Q. Liang, J. Li, H. He, W. Liang, T. Zhang, X. Fan, *Front. Environ. Sci. Eng.* **2017**, *11*, 4.
- [8] a) J. Tan, C. Solbrig, S. J. Schmiege, *SAE Int.* **2011**, *2011*, 2001–1140; b) M. Naseri, S. Chatterjee, M. Castagnola, H.-Y. Chen, J. Fedeyko, H. Hess, J. Li, *SAE Int. J. Engines* **2011**, *4*, 1798–1809; c) K. Johansen, A. Widd, F. Zuther, H. Viecz, *SAE [Tech. Pap.]* **2016**, 0148–7191.
- [9] K. Johansen, H. Bentzer, A. Kustov, K. Larsen, T. V. Janssens, R. G. Barfod, *SAE [Tech. Pap.]* **2014**, 0148–7191.
- [10] a) L. Chen, J. Li, M. Ge, *J. Phys. Chem. C* **2009**, *113*, 21177–21184; b) M. Shen, L. Xu, J. Wang, C. Li, W. Wang, J. Wang, Y. Zhai, *J. Rare Earth.* **2016**, *34*, 259–267.
- [11] R. Gao, D. Zhang, X. Liu, L. Shi, P. Maitarad, H. Li, J. Zhang, W. Cao, *Catal. Sci. Technol.* **2013**, *3*, 191–199.
- [12] a) J. M. Christensen, J.-D. Grunwaldt, A. D. Jensen, *Appl. Catal. B* **2016**, *188*, 235–244; b) J. Beckers, G. Rothenberg, *Green Chem.* **2010**, *12*, 939–948; c) T. Garcia, B. Solsona, S. H. Taylor, *Appl. Catal. B* **2006**, *66*, 92–99; d) M. Tepluchin, M. Casapu, A. Boubnov, H. Lichtenberg, D. Wang, S. Kureti, J.-D. Grunwaldt, *ChemCatChem* **2014**, *6*, 1763–1773; e) D. Reichert, H. Bockhorn, S. Kureti, *Appl. Catal. B* **2008**, *80*, 248–259; f) S. Wagloehner, S. Kureti, *Appl. Catal. B* **2012**, *125*, 158–165; g) C. He, J. Cheng, X. Zhang, M. Douthwaite, S. Pattison, Z. Hao, *Chem. Rev.* **2019**, *119*, 4471–4568.
- [13] B. M. Reddy, A. Khan, Y. Yamada, T. Kobayashi, S. Loidant, J.-C. Volta, *J. Phys. Chem. B* **2003**, *107*, 5162–5167.
- [14] J. Liu, Z. Zhao, C. Xu, J. Liu, *Chin. J. Catal.* **2019**, *40*, 1438–1487.
- [15] B. Solsona, T. Garcia, R. Sanchis, M. Soriano, M. Moreno, E. Rodríguez-Castellón, S. Agouram, A. Dejoz, J. L. Nieto, *Chem. Eng. J.* **2016**, *290*, 273–281.
- [16] a) E. Japke, M. Casapu, V. Trouillet, O. Deutschmann, J.-D. Grunwaldt, *Catal. Today* **2015**, *258*, 461–469; b) L. Zheng, M. Casapu, M. Stehle, O. Deutschmann, J.-D. Grunwaldt, *Top. Catal.* **2018**, *62*, 129–139; c) M. Koebel, M. Elsener, *Ind. Eng. Chem. Res.* **1998**, *37*, 3864–3868.
- [17] T. Srnak, J. Dumesic, B. Clausen, E. Törnqvist, N.-Y. Topsøet, *J. Catal.* **1992**, *135*, 246–262.

- [18] a) U. Balachandran, N. Eror, *J. Solid State Chem.* **1982**, *42*, 276–282; b) O. Frank, M. Zukalova, B. Laskova, J. Kürti, J. Koltai, L. Kavan, *Phys. Chem. Chem. Phys.* **2012**, *14*, 14567–14572.
- [19] a) V. Panchal, S. López-Moreno, D. Santamaría-Pérez, D. Errandonea, F. Manjón, P. Rodríguez-Hernandez, A. Muñoz, S. Achary, A. Tyagi, *Phys. Rev. B* **2011**, *84*, 024111; b) R. Rao, A. B. Garg, B. Wani, *J. Phys. Conf. Ser.* **2012**, *377*, 012010.
- [20] K. Routray, W. Zhou, C. J. Kiely, I. E. Wachs, *ACS Catal.* **2010**, *1*, 54–66.
- [21] G. T. Went, S. T. Oyama, A. T. Bell, *J. Phys. Chem.* **1990**, *94*, 4240–4246.
- [22] a) L. D. Arsov, C. Kormann, W. Plieth, *J. Raman Spectrosc.* **1991**, *22*, 573–575; b) H. Ma, J. Yang, Y. Dai, Y. Zhang, B. Lu, G. Ma, *Appl. Surf. Sci.* **2007**, *253*, 7497–7500.
- [23] K. Bhattacharyya, S. Varma, A. Tripathi, S. Bharadwaj, A. Tyagi, *J. Phys. Chem. C* **2008**, *112*, 19102–19112.
- [24] P. A. Kumar, Y. E. Jeong, S. Gautam, H. P. Ha, K. J. Lee, K. H. Chae, *Chem. Eng. J.* **2015**, *275*, 142–151.
- [25] A. Boubnov, H. Lichtenberg, S. Mangold, J.-D. Grunwaldt, *J. Synchrotron Radiat.* **2015**, *22*, 410–426.
- [26] a) M. Wilke, G. M. Partzsch, R. Bernhardt, D. Lattard, *Chem. Geol.* **2005**, *220*, 143–161; b) J. Liu, L. Wang, F. Okejiri, J. Luo, J. Zhao, P. Zhang, M. Liu, S. Yang, Z. Zhang, W. Song, *ACS Catal.* **2020**, *10*, 8950–8959.
- [27] R. Häggblad, S. Hansen, L. R. Wallenberg, A. Andersson, *J. Catal.* **2010**, *276*, 24–37.
- [28] Y.-F. Y. Yao, *Ind. Eng. Chem. Prod. Res. Dev.* **1980**, *19*, 293–298.
- [29] R. Jossen, M. C. Heine, S. E. Pratsinis, S. M. Augustine, M. K. Akhtar, *Appl. Catal. B* **2007**, *69*, 181–188.
- [30] T. C. Watling, Y. Lopez, J. D. Pless, B. Sukumar, W. Klink, P. Markatou, *SAE Int. J. Engines* **2013**, *6*, 882–897.
- [31] a) M. Casapu, O. Kröcher, M. Mehring, M. Nachttegaal, C. Borca, M. Harfouche, D. Grolimund, *J. Phys. Chem. C* **2010**, *114*, 9791–9801; b) K. A. Michalow-Mauke, Y. Lu, D. Ferri, T. Graule, K. Kowalski, M. Elsener, O. Kröcher, *Chimia* **2015**, *69*, 220–224.
- [32] A. Cavaliere, R. Barbella, A. Ciajolo, A. D’anna, R. Ragucci, *Symp. (Int.) Combust.* **1994**, *25*, 167–174.
- [33] M. Bokova, C. Decarne, E. Abi-Aad, A. Pryakhin, V. Lunin, A. Aboukais, *Thermochim. Acta* **2005**, *428*, 165–171.
- [34] B. R. Stanmore, J.-F. Brillhac, P. Gilot, *Carbon* **2001**, *39*, 2247–2268.
- [35] R. Cousin, S. Capelle, E. Abi-Aad, D. Courcot, A. Aboukais, *Appl. Catal. B* **2007**, *70*, 247–253.
- [36] J. Schobing, V. Tschamber, J.-F. Brillhac, A. Auclair, Y. Hohl, C. R. Chim. **2018**, *21*, 221–231.
- [37] J. P. Neeft, M. Makkee, J. A. Moulijn, *Appl. Catal. B* **1996**, *8*, 57–78.
- [38] a) I. C. L. Leocadio, S. Braun, M. Schmal, *J. Catal.* **2004**, *223*, 114–121; b) J. Liu, Z. Zhao, C. Xu, A. Duan, L. Zhu, X. Wang, *Appl. Catal. B* **2005**, *61*, 36–46.
- [39] a) B. Marchon, J. Carrazza, H. Heinemann, G. Somorjai, *Carbon* **1988**, *26*, 507–514; b) B. Marchon, W. Tysoe, J. Carrazza, H. Heinemann, G. Somorjai, *J. Phys. Chem.* **1988**, *92*, 5744–5749.
- [40] A. Zimina, K. Dardenne, M. Denecke, D. Doronkin, E. Huttel, H. Lichtenberg, S. Mangold, T. Pruessmann, J. Rothe, T. Spangenberg, J.-D. Grunwaldt, *Rev. Sci. Instrum.* **2017**, *88*, 113113.
- [41] T. Spangenberg, J. Göttlicher, R. Steininger, in: *AIP Conference Proceedings, Vol. 1092*, American Institute of Physics, **2009**, pp. 93–97.
- [42] B. Ravel, M. Newville, *J. Synchrotron Radiat.* **2005**, *12*, 537–541.
- [43] J. M. Christensen, J.-D. Grunwaldt, A. D. Jensen, *Appl. Catal. B* **2017**, *205*, 182–188.

Manuscript received: August 12, 2020

Revised manuscript received: September 9, 2020

Accepted manuscript online: September 17, 2020

Version of record online: October 15, 2020